An All-Optically Controlled Liquid-Crystal Plasmonic Metasurface Platform

Mukesh Sharma and Tal Ellenbogen*

The need for thin active metasurface based elements, opens an exciting research direction toward exploration of various active materials and their control mechanisms. Here, an all-optical control mechanism of composite metasurfaces is studied, based on rapid laser-induced thermo-optical nonlinearities in nematic liquid crystals (NLCs). Specifically, the absorption of photons leads to local heating, which in turn facilitates a nematic-to-isotropic (N–I) phase transition of a twisted-NLC (TNLC) layer that is sandwiched between an indium tin oxide (ITO) coated glass plate and the metasurface. This mechanism is used to experimentally demonstrate all-optically switchable plasmonic metasurface color tag. The dependence of the switching on the laser power and the dynamic response of the device are characterized. Experimental results show that the pump beam power significantly affects the switching time, which can be further reduced by thermal management of the design. Such switching mechanisms have great potential in all-optically controlled systems and can be applied to realize additional active and multifunctional optical devices at nanoscale.

1. Introduction

The development of active metasurfaces, together with their tunable optical response, are providing a new platform for reconfigurable optical devices at the nanoscale.[1–8] To achieve such devices, a number of active materials and active control techniques, have emerged based on electrical, mechanical, thermal, and optical mechanisms.[9–18] In particular, all-optical switching mechanisms are attractive as they can potentially overcome the limitations of electronics, and may be important for the development of ultrafast reconfigurable platforms.

Reconfigurable nematic liquid crystals (NLCs) based metasurfaces attracted a great deal of attention lately.[19–28] This is due to reaction of the LC molecules to numerous external stimuli such as light, temperature, and electric or magnetic fields,[29–32] in addition to their high birefringence and broadband response over the entire visible–IR–THz–microwave spectrum.[31] For applications of all-optical switching, light-induced nematic-to-isotropic (N–I) phase transition via local heating (i.e., change in refractive index and order parameter), has been proposed and studied.[31–37]

The local heating of the NLC is mediated through the absorption of photons energy which is then thermally dissipated. Beyond a threshold input power, the local temperature becomes higher than the critical temperature required for N–I phase transition. It has been reported that laser-induced thermal effects in NLC enable relatively rapid switching times when the local heating is realized by short laser pulses.[31,33–36,38] By exploiting this interesting switching mechanism, it is possible to realize highly tunable and efficient active metasurface-based devices such as phase-shifters, optical switches, modulators, and sensors. For example, it can be employed to actively control the fundamental localized surface plasmon resonance (LSPR) in an integrated LC-plasmonic metasurface system. In plasmonic metasurfaces, the LSPR is strongly dependent on the structural shape and size of the nanostructure, the polarization of incoming light, and the surrounding dielectric medium.[39] Therefore, the LSPR wavelength can be modified abruptly using such thermo-optical switching mechanism, either by changing the refractive index of the LC, or by rotating the polarization of incident light.

Recently, Pietro et al.[38] experimentally demonstrated a strong spatial self-phase modulation by exploiting ultrashort laser-induced thermal nonlinearity in E7 NLCs. This preliminary study represented a new insight for application of thermally-induced nonlinearities in NLCs and was used as a means to achieve beam shaping. Yet, nonlinear thermal effects via local optical heating of NLCs in a controllable manner provide a much wider range of interesting opportunities. Specifically, using these effects as means to achieve active control of metasurfaces may lead to a plethora of new optical devices. Here, we demonstrate a novel LC-metasurface device configuration that can be all-optically controlled by exploiting the thermo-optical nonlinearities in NLCs. We specifically use the optically induced N–I phase transition for polarization switching in a twisted-NLC (TNLC) layer, which

Dr. M. Sharma, Prof. T. Ellenbogen
Department of Physical Electronics
Faculty of Engineering
Tel-Aviv University
Tel-Aviv 6779801, Israel
E-mail: mukeshsharma@mail.tau.ac.il
Dr. M. Sharma, Prof. T. Ellenbogen
Center for Light-Matter Interaction
Tel-Aviv University
Tel-Aviv 6779801, Israel

The ORCID identification number(s) for the author(s) of this article can be found under https://doi.org/10.1002/lpor.202000253

DOI: 10.1002/lpor.202000253

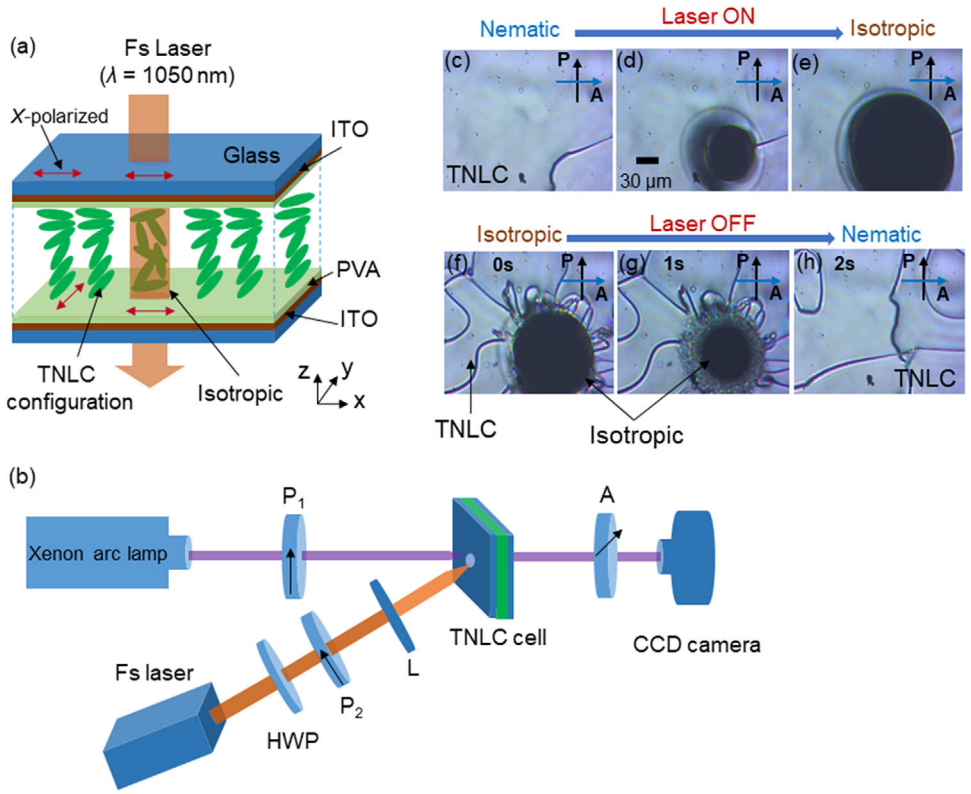

Figure 1. a) Illustration of the TNLC cell and schematic representation of N–I phase transition with application of NIR (λ = 1050 nm) femtosecond (fs) laser pulses. The region of TNLC configuration rotates the polarization of incident *x*-polarized light by 90° and the isotropic region, induced by laser pulses, does not rotate the polarization of light. b) Schematic illustration of the experimental setup. Xenon arc lamp (white light), Fs laser (Ti–Sapphire laser, ≈140 fs pulse length, 80 MHz repetition rate, λ = 1050 nm), half-wave plate (HWP), polarizer (P_2), lens (L) (F = 100 mm), polarizer (P_1), analyzer (A), and CCD camera. c) Snapshots of the micrographic textures of the TNLC cell before impinging laser pulses, d,e) while switching laser on and slowly increasing its power. f–h) Snapshots of the TNLC cell at different times after the laser is switched-off. The I–N phase transition is observed and the TNLC configuration is restored.

in turn controls the interaction with the plasmonic metasurface. Employing this tuning mechanism, an active LC-plasmonic metasurface platform based color tag "TAU" is demonstrated. The polarization-selective transmitted colors of the active tag are dynamically controlled by using the laser pulses. The switching is characterized in terms of threshold laser power, hysteresis behavior, and measurement of the dynamic response time by using pump-probe technique.

2. Results and Discussion

2.1. Polarization Switching by Optically Induced Phase Transition

Figure 1a illustrates the schematic diagram of the proposed nonlinear all-optical switching configuration of the TNLC cell. The NLC used in the cell was 4′-*n*-pentyl-4-cyanobiphenyl (5CB) which has the N–I phase transition at a clearing temperature T_c ≈ 308 K.[31] To induce the TNLC configuration a standard clean-room fabrication procedure (see Experimental Section) was performed. In this configuration, the incident polarization of light follows 90° rotation of the director axis, as long as the cell is satisfying the Mauguin's condition.[40] By applying NIR femtosecond (fs) laser pulses (Ti–Sapphire laser, 140 fs, 80 MHz, λ = 1050 nm) the order parameter can be changed to switch the system from nematic to isotropic phase. The laser-induced phase transition provides two different regions inside the device (see Figure 1a): one region, outside the interaction area, keeps the TNLC configuration which rotates the incident polarization of light by 90°, while another region (area of focused spot [diameter ≈ 66 μm]) becomes isotropic due to the phase transition. In this region the polarization of light does not rotate. Thus, such thermo-optic effect provides the key to obtain highly localized, micron scale, and all-optical switching in a controllable manner.

Next, we experimentally demonstrate the switching mechanism in the fabricated TNLC cell by analyzing the transmission of linearly polarized white light (Xenon arc lamp) through the two different regions when the cell is placed between crossed polarizer and analyzer. Schematic of the experimental setup is shown in Figure 1b. The pump pulses are focused by a lens (L) (F = 100 mm) on the TNLC cell. The power of the pump pulses can be continuously adjusted by using a half wave plate and a polarizer. The output white light is captured by a CCD camera. Snapshots of the micrographic textures of the TNLC cell, captured at different times, are shown in Figure 1c–h. Figure 1c shows the surface before impinging laser pulses on the device. Figure 1d,e shows the laser-induced N–I phase transition at increasing laser powers. The real-time experimental demonstration of phase transition is shown in Movie S1, Supporting Information. The N–I phase

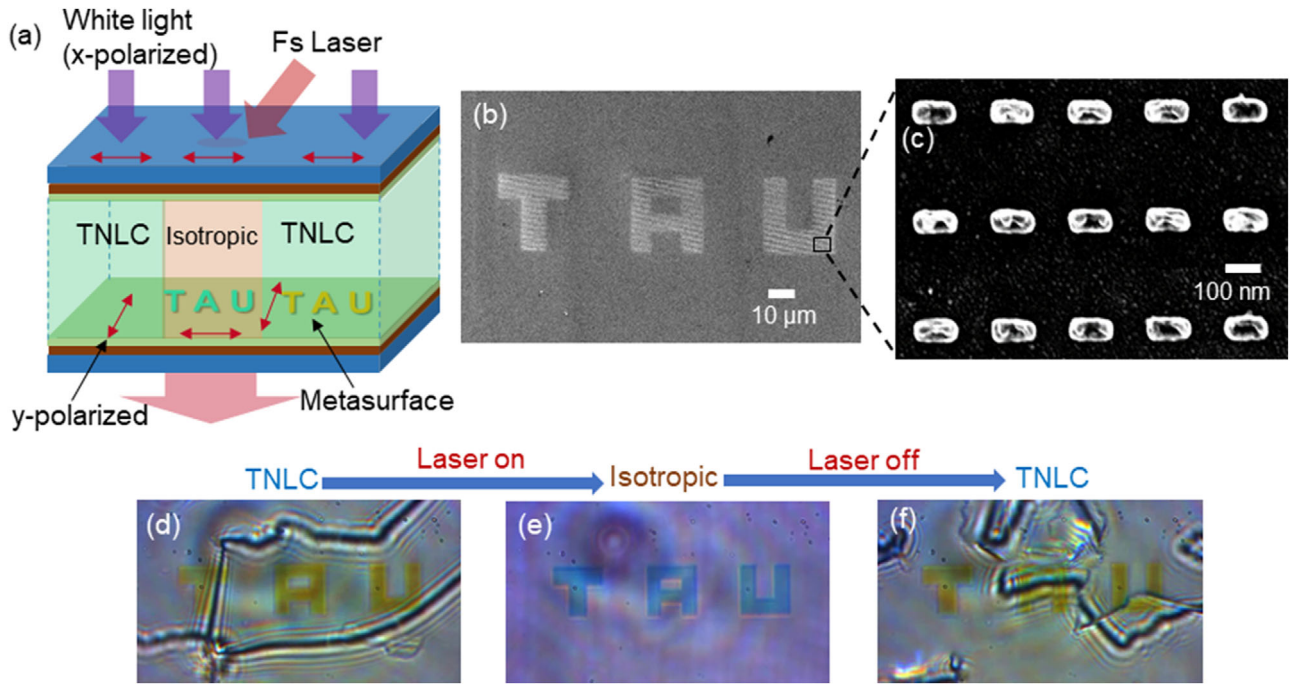

Figure 2. Demonstration of the thermo-optical switching mechanism on the active LC-plasmonic metasurface device. a) Schematic view of the active "TAU" color tag. The TNLC region rotates the polarization of incident *x*-polarized light by 90° and converts it to *y*-polarized light that excites the corresponding LSPR. The laser-induced isotropic region does not rotate the polarization of incident *x*-polarized light. SEM images of b) rod-shaped nanoantennas array based TAU tag with scale bar of 10 μm and c) rod-shaped nanoantennas array with scale bar of 100 nm, respectively. Transmission images of TAU tag, d) for incident *x*-polarized light when laser is off (yellow color), e) isotropic phase transition occurs when laser is on (blue color), f) TNLC configuration is restored when laser is off.

transition is observed at threshold input power $P_{in} \approx 62$ mW. During N–I phase transition, the laser illuminated area (focal spot size ≈ 66 μm) became dark due to the transition to isotropic state that does not rotate the polarization of light, which is then blocked by the crossed analyzer. The non-illuminated area stays in the TNLC configuration which continues to transmit the white light through the analyzer. It was observed that the isotropic region becomes wider with increasing laser powers (Figure 1d,e). Figure 1f–h shows the microscopic changes in the textures at different times during the I–N phase transition when laser is switched-off. The granular pattern is observed due to rapid domain formation in intermediate backward phase transition. Finally, the TNLC configuration is restored again which results in white light transmission through the crossed polarizers condition.

2.2. All-Optically Switchable Plasmonic Metasurface Color Tag

We use this laser-induced thermo-optical effect to experimentally demonstrate an all-optically switchable metasurface based color tag. The metasurface is constructed from 50 nm thick rod-shaped aluminum nanoantenna arrays. The metasurface is fabricated by using standard electron-beam lithography process (see Experimental Section). Each rod nanoantenna in the metasurface is 120 nm long, 50 nm wide, and the lattice spacing is 200 and 250 nm on horizontal and vertical directions, respectively. In order to make an active metasurface tag, a TNLC layer (thickness of 6 μm) is integrated over the metasurface, which is sandwiched between two ITO-coated glass plates, as shown in **Figure 2**a. Each of the glass plates is coated with a PVA alignment layer with thickness of ≈100 nm and rubbed in orthogonal relative direction to achieve 90° twist of the director axis of LC molecules from bottom to top inner surfaces. Figure 2b,c shows the scanning electron microscope (SEM) images of the fabricated TAU tag and corresponding constructed unit of rod-shaped nanoantennas, respectively. Figure 2d shows the transmission image of active TAU tag for *x*-polarized light. It can be seen that the incident *x*-polarized light, first, is rotated about 90° by the TNLC layer, then it interacts with short axes (along the width of 50 nm) of the rod-shaped nanoantennas, and excites LSPR at shorter wavelength and the TAU tag looks yellow in transmission (see Figure 2a,d).

By turning on the switching laser we can control the color of the metasurface tag. The real-time experimental demonstration is shown in Movie S2, Supporting Information. When the NIR laser, above a threshold power, is focused to the area on the device containing the TAU tag, the N–I phase transition is induced. Therefore, the TNLC configuration disappears and there is no more rotation of the plane of polarization of incoming light in this specific region (see Figure 2e). In this case, incident *x*-polarized light, that is parallel to the long axes (along the length of 120 nm) of the nanoantennas array, excites LSPR at longer wavelength which corresponds to observe blue color in transmission (see Figure 2e). Again, when the laser is switched-off the TNLC configuration is restored due to I–N phase transition and the transmitted colors of the TAU tag change back from blue to

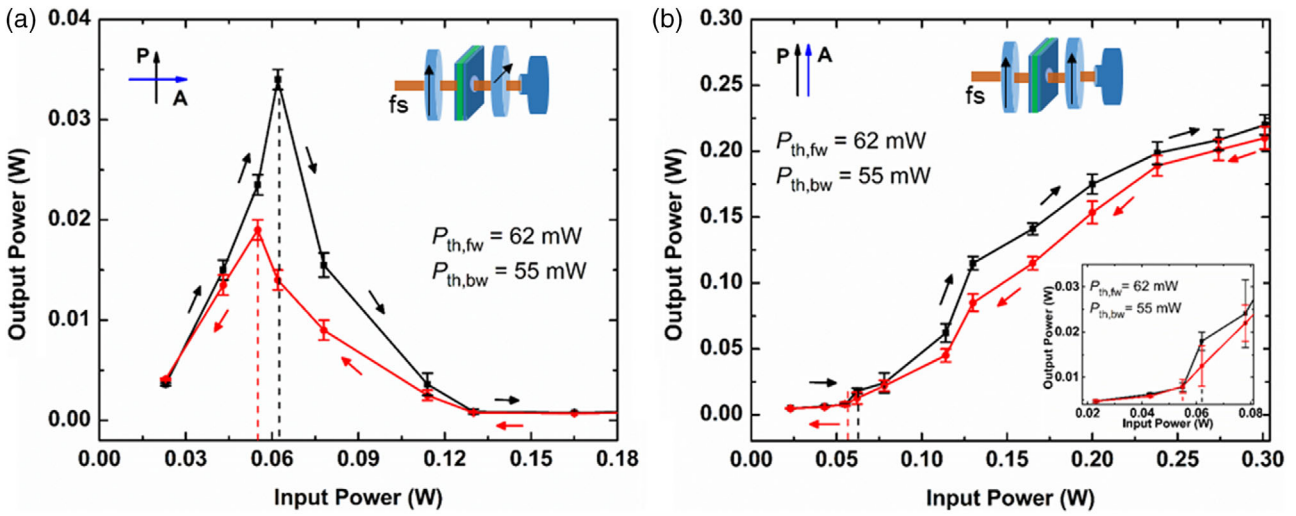

Figure 3. The variation in output power with input power in forward and backward direction for both a) crossed and b) parallel polarizer and analyzer conditions, respectively. Insets: Schematic of the experimental setup and the zoomed region at low values of input power in inset of (b).

yellow (see Figure 2f). Thus, polarization switching by LC phase transition enables excitation of different LSPR of the metasurface. In addition, by doing the experiment multiple times it was observed that the switchable device shows excellent reliability and repeatability. In this experiment, the incident polarization was fixed at *x*-polarized light and only the laser was switched on and off periodically. By using more complex polarization structure of the light or the metasurface tag it is possible to demonstrate simultaneously multiple and independent localized color tags on the same device.

2.3. Nonlinear Optical Characterization

To characterize the nonlinear behavior, two experimental measurements were performed on the TNLC cell. In the first experiment, the TNLC cell was placed between crossed polarizer and analyzer (see inset of **Figure 3**a) whereas in the other experiment, it was placed between parallel polarizer and analyzer (see inset of Figure 3b). For the nonlinear characterization, we used only the femtosecond laser, which was focused at normal incidence into the TNLC cell by a lens ($F = 100$ mm) and the output power was measured as function of the input power. Here, it is mentioned that all measurements were taken after the LC system reached its thermal equilibrium. Figure 3a presents the results for the crossed polarizers configuration. It can be seen that in the forward direction (while slowly increasing the local heating induced by the laser), before the threshold, the transmitted power shows linear dependence on the input power. After a threshold power $P_{in,fw} = 62$ mW, the transmitted light begins to drop dramatically. This is due to the optically induced temperature rise in the LC layer from $T_{ambient}$ (≈297 K) to T_c (≈308 K), which leads to N–I phase transition. In the isotropic state the transmission of light is blocked by crossed polarizer and analyzer, as expected (see Figure 1b–d). This temperature rise can be estimated by $\Delta T = Q / \rho C_p$,[41] where, ρ and C_p are the density and the specific heat of 5CB LC, and Q is the generated heat density due to the absorption of input power by the LC. The absorbed power can be calculated by using the relation $P_{ab} = P_{in}\,(1 - e^{-\alpha d})$, where α and d are the absorption coefficient and thickness of the LC, respectively. The generated heat density is estimated by $Q = P_{ab} / (\pi r_o^2 d)$, where, $\pi r_o^2 d$ is the approximated interaction volume. By using the parameters, $P_{in} = 62$ mW, $r_o = 33$ µm, $\alpha = 8$ m^{-1},[35] $\rho_{LC} = 1.02 \times 10^3$ kg m^{-3}, $C_{p,LC} = 1.92 \times 10^3$ J kg^{-1} K^{-1},[31] we obtain $P_{ab} \approx 3$ µW and $\Delta T \approx 75$ K. This value shows that in principal the absorbed light is capable of heating the 5CB LC above its clearing temperature. However, due to the diffusion of heat through the ITO layers, which are much better thermal conductors than the 5CB LC, the actual temperature rise of the LC is only of ≈11 K in this case. The variation in the transmitted power in the backward direction (during cooling when laser power is reduced) reveals hysteresis (as reported before in the literature)[30] and the threshold laser power is reduced to $P_{in,bw} = 55$ mW. Such hysteresis properties can be very important for realizing various devices such as optical logic gates, optical memories, and optical switches.

Figure 3b shows the variation in the transmitted power with respect to input power when TNLC cell is placed between two parallel polarizers. One can see from Figure 3b, that the TNLC cell shows almost zero transmission at low input power. After crossing the forward direction threshold laser power of $P_{in,fw} =$ 62 mW, a nonlinear increase of the transmitted power with respect to the input power is observed (see inset of Figure 3b). This behavior is also due to the onset of N–I phase transition at the threshold, which increases the maximum light transmission through the isotropic medium in between the parallel polarizers. Also here the hysteresis behavior is clearly observed when reducing the power down.

2.4. Dynamic Switching Response

We also studied the response time of the system using different pump powers. Schematic of the experimental setup is shown in **Figure 4**a (see also Experimental Section). A continuous wave

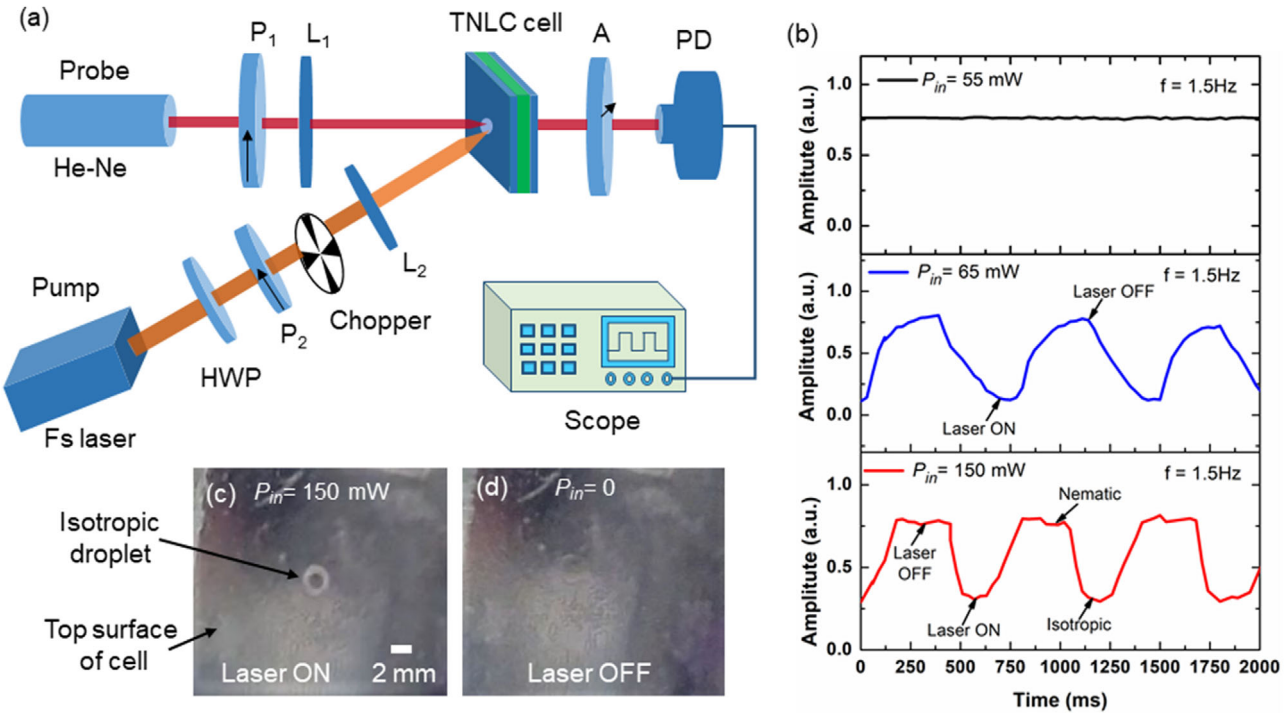

Figure 4. a) Schematic diagram of the pump-probe experimental setup. b) Response time of the device at different input switching (pump) laser powers $P_{in} = 55$ mW, $P_{in} = 65$ mW, and $P_{in} = 150$ mW. The rise and fall times are decreased as switching laser power increases. Snapshots of the top surface of device c) when laser is illuminated at $P_{in} = 150$ mW (laser ON state) d) when $P_{in} = 0$ (laser OFF state). The formation of isotropic droplet-like structure is observed when laser is switched-on. The scale bar is 2 mm.

He–Ne laser with wavelength of 633 nm and the femtosecond laser were used as probe beam and pump beam, respectively. The time response of the system has been measured by chopping the pump beam before the device with a controlled optical chopper. Figure 4b shows the time response of the device at a fixed optical chopper frequency $f = 1.5$ Hz, for three different cases of pump beam powers of $P_{in} = 55$ mW, $P_{in} = 65$ mW, and $P_{in} = 150$ mW. It is observed that there is almost no change in the probe beam output when the pump beam power is below threshold ($P_{in} = 55$ mW) (see also Figure 4b) as the LC is in its nematic phase and the TNLC configuration rotates the polarization of the probe. A transient response following the chopper frequency is observed when the pump beam power passes threshold ($P_{in} = 62$ mW) with the formation of isotropic droplet-like structure due to N–I phase transition (see Movie S3, Supporting Information). Figure 4c,d shows the macrographical textures of top surface of the TNLC cell with a fixed pump beam power of $P_{in} = 150$ mW and $P_{in} = 0$, respectively. Also, the isotropic droplet appears and disappears simultaneously with pump laser on and off states (see Movie S3, Supporting Information).

The response times of switching are measured as ≈180 ms (rise edge) and ≈240 ms (fall edge) at pump beam power of $P_{in} = 65$ mW. At higher value of pump power of $P_{in} = 150$ mW, the response times are reduced to ≈125 ms (rise edge) and ≈60 ms (fall edge). One can see that the measured response time for switching is on the order of milliseconds, which is in the typical range of thermal effects in NLCs based devices.[31,42] Therefore, it also qualitatively matches our interpretation of a thermal origin of the effect. Here, it is mentioned that the measured response time of the TNLC cell is slower than that of other active devices made by using different active materials.[5–7,16] In general, the response time of nematic LCs is obtained in the range between milliseconds to seconds (at modulation frequencies up to kHz) at a relatively low power consumption, whereas a faster response, in the range of sub-microseconds (at MHz modulation frequency) can be achieved by using other active materials.[7] However, this measured response time could be further reduced by considering thermal management of the system. Since thermal buildup is critical for the optical switching, it also strongly depends on the thickness of the TNLC cell, beam spot size, the absorption coefficients, and the thermal conductivities of all materials (glass/ITO/PVA/5CB LC). Here, we mention that the resolution or the smallest pitch size that can be controlled by this mechanism is strongly dependent on the response time and the heat diffusion area (or rate of heat diffusion). The measured response time for switching is on the order of milliseconds whereas the thermal diffusion-relaxation time ($\tau_{dif} \approx D^{-1}(1/r_o^2 + \pi^2/d^2)^{-1}$)[35] for 5CB LC ($D \approx 10^{-3}$ cm^2 s^{-1}, $r_o = 33$ µm and $d = 6$ µm; where D is the diffusion constant) is estimated as $\tau_{dif} \approx 36$ µs, which is in microsecond time scale. Since, the thermal diffusion-relaxation time is faster than the measured switching time, hence, the resolution is primarily limited by the heat diffusion area rather than laser illuminated area. Taking the harsh assumption that the diffused heat spot will limit the pitch, we can estimate its diameter by $d_{spot} = 2 \times \sqrt{D \times t_{response}/\pi}$. For response time in our case of ≈100 ms this gives a value of ≈100 µm pitch, which can go down

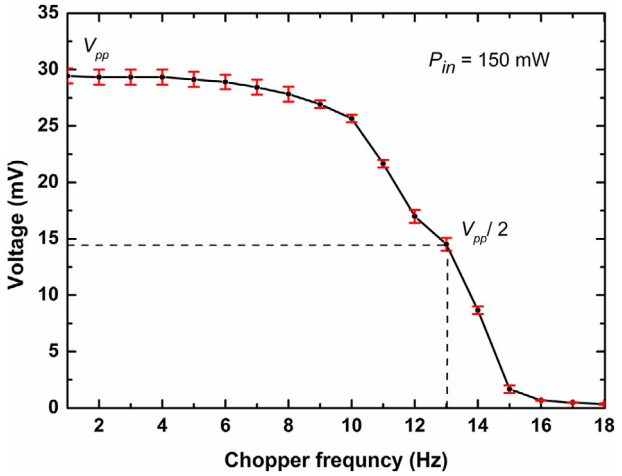

Figure 5. Variation in probe beam amplitude with chopper frequencies at a fixed laser power P_{in} = 150 mW.

to 10 μm for 1 ms response time. However, if one would like to switch a single spot, then its size can be much smaller than that.

We also measured the frequency response of the device by varying the chopper frequency at a fixed laser power P_{in} = 150 mW, and measuring the peak to peak voltage on the detector (see **Figure 5**). It can be seen that the amplitude of the modulation of the probe beam is reduced with increasing chopper frequencies between 0–18 Hz. From this measurement the switching bandwidth can be obtained to be ≈13 Hz, which agrees well with the rise and fall times shown in Figure 4b.

3. Conclusions

We have experimentally demonstrated an all-optically switchable metasurface color tag device. The switching is based on nonlinear thermo-optic polarization switching in a TNLC cell, controlled by laser-induced phase transition in the NLCs. We show that the origin of the phase transition is achieved by local heating of the TNLC layer. We further measure the response time by using pump-probe technique. We show that it is in the 100 ms regime and it is dependent on the pump power, which can increase the heating rate and reduce the switching time. This response time can be further reduced by proper thermal design of the device. Another promising direction to explore is to tune the switch beam to excite the metasurfaces in their plasmon resonances and exciting localized thermo-plasmonic effects,[43,44] which will lead to highly local and potentially much faster phase transitions. With the growing interest in active metasurfaces, such switching mechanisms show great potential for all-optical control and can be further exploited in developing various active optical devices in the future.

4. Experimental Section

Fabrication of TNLC Cell: Two indium tin oxide (ITO) coated glass substrates (30 nm thick ITO layer, Sigma-Aldrich) were cleaned and spin-coated with an alignment layer of PVA (≈100 nm thickness), followed by baking at 120 °C for 30 min. After cooling at room temperature, the baked PVA layers were rubbed in orthogonal directions by using a soft velvet cloth. This rubbing process allowed to promote a TNLC configuration of the 5CB LC molecules in the cell. A 6 μm thick Mylar spacer layer (Sigma-Aldrich) was used between substrates and then it was assembled together by using UV-curable adhesive NOA61 followed by UV curing. The nematic 5CB LC was infiltrated into cell by capillary action. During the LC infiltration procedure, the fabricated device was kept on a hot plate which maintained temperature of 50 °C. At this temperature, the 5CB LC was in its isotropic phase, which had lower viscosity than its nematic phase, and therefore it could be easily infiltrated into the gap.

Fabrication of Hybrid LC-Plasmonic Metasurface Based TAU Tag: The plasmonic metasurface based TAU tag, consisting of a periodic array of rod-shaped aluminum (Al) nanoantennas, was fabricated by using standard electron-beam lithography technique (using Raith 150 II). The period of the nanoantenna arrays was 200 and 250 nm on horizontal and vertical directions, respectively, and the thicknesses of the ITO layer and the Al layer were 30 and 50 nm, respectively. At first, an ITO-coated glass substrate with ITO layer thickness of 30 nm (Sigma-Aldrich) was cleaned, spin-coated with a photoresist poly (methyl methacrylate) (PMMA), and baked at 180 °C on a hot plate for 2 min. After developing the pattern, an Al layer of thickness 50 nm was deposited by evaporation, followed by a lift-off process. The substrate with the TAU tag was spin-coated with an alignment layer of PVA (≈100 nm thickness). Another ITO-coated glass substrate was spin-coated with the same alignment layer of PVA (≈100 nm thickness). Both PVA-coated substrates were baked at 120 °C for 30 min and subsequently cooled to room temperature. The baked PVA layers were then rubbed mechanically in the orthogonal directions to each other to promote a TNLC configuration of LC molecules. After this the same procedure was followed up to infiltration of 5CB LC inside the device explained in section of fabrication of TNLC cell.

Experimental Setups: A femtosecond Ti–Sapphire laser (Chameleon Ultra), was used as the pump laser. The laser generated the NIR femtosecond laser pulses, with center wavelength of λ = 1050 nm, 140 fs pulse duration, and high repetition rate of 80 MHz. In the experiment of response time measurement, a low frequency optical chopper (Stanford Research Systems SR540) was used to modulate the pump laser. The TNLC cell was placed between crossed or parallel polarizer and analyzer. The intensity of the probe beam (He–Ne laser with wavelength of 633 nm) was kept constant and the focused spot size of the pump was kept larger than the probe so that the whole probe beam passed through the spot of the pump beam. The probe beam output signal was detected by a Silicon photo detector and output time response was recorded on an oscilloscope (Tektronix TDS1002). In addition, the optical transmission images of the illuminated tags area were captured by a color camera that was placed after the analyzer.

Supporting Information

Supporting Information is available from the Wiley Online Library or from the author.

Acknowledgements

This research was supported by the Israeli Ministry of Science and Technology grant agreement no. 3-15614. The authors would like to thank Dr. Netta Hendler for help during the fabrication process of plasmonic metasurface, and Lior Michaeli and Dr. Shivani Bhardwaj for their constructive suggestions. M.S. acknowledges the support from the Israeli Ministry of Science and Technology for the Postdoc Fellowship.

Conflict of Interest

The authors declare no conflict of interest.

Keywords

all-optical control systems, liquid crystals, localized surface plasmons, plasmonic metasurfaces, thermo-optic nonlinearity, tunable color devices

Received: June 18, 2020
Revised: September 9, 2020
Published online: September 23, 2020

[1] A. M. Shaltout, V. M. Shalaev, M. L. Brongersma, *Science* **2019**, *364*, 648.
[2] L. Kang, R. P. Jenkins, D. H. Werner, *Adv. Opt. Mater.* **2019**, *7*, 1801813.
[3] Q. Ma, G. D. Bai, H. B. Jing, C. Yang, L. Li, T. J. Cui, *Light: Sci. Appl.* **2019**, *8*, 98.
[4] C. W. Lee, H. J. Choi, H. Jeong, *Nano Convergence* **2020**, *7*, 3.
[5] H. T. Chen, A. J. Taylor, N. Yu, *Rep. Prog. Phys.* **2016**, *79*, 076401.
[6] A. Forouzmand, M. M. Salary, S. Inampudi, H. Mosallaei, *Adv. Opt. Mater.* **2018**, *6*, 1701275.
[7] Y. W. Huang, H. W. H. Lee, R. Sokhoyan, R. A. Pala, K. Thyagarajan, S. Han, D. P. Tsai, H. A. Atwater, *Nano Lett.* **2016**, *16*, 5319.
[8] A. Forouzmand, M. M. Salary, G. K. Shirmanesh, R. Sokhoyan, H. A. Atwater, H. Mosallaei, *Nanophotonics* **2019**, *8*, 415.
[9] J. Sautter, I. Staude, M. Decker, E. Rusak, D. N. Neshev, I. Brener, Y. S. Kivshar, *ACS Nano* **2015**, *9*, 4308.
[10] M. X. Ren, W. Wu, W. Cai, B. Pi, X. Z. Zhang, J. J. Xu, *Light: Sci. Appl.* **2017**, *6*, e16254.
[11] Y. Wang, Y. Guo, H. Liao, Z. Li, F. Gan, C. Sun, J. Chen, *ACS Photonics* **2018**, *5*, 1575.
[12] S. V. Makarov, A. S. Zalogina, M. Tajik, D. A. Zuev, M. V. Rybin, A. A. Kuchmizhak, S. Juodkazis, Y. Kivshar, *Laser Photonics Rev.* **2017**, *11*, 1700108.
[13] G. Grinblat, R. Berté, M. P. Nielsen, Y. Li, R. F. Oulton, S. A. Maier, *Nano Lett.* **2018**, *18*, 7896.
[14] A. E. Minovich, A. E. Miroshnichenko, A. Y. Bykov, T. V. Murzina, D. N. Neshev, Y. S. Kivshar, *Laser Photonics Rev.* **2015**, *9*, 195.
[15] M. M. Shanei, D. Fathi, F. Ghasemifard, O. Quevedo-Teruel, *Sci. Rep.* **2019**, *9*, 13641.
[16] A. Nemati, Q. Wang, M. Hong, J. Teng, *Opto-Electron. Adv.* **2018**, *1*, 18000901.
[17] F. Kurtz, C. Ropers, G. Herink, *Nat. Photonics* **2020**, *14*, 9.
[18] K. Thyagarajan, R. Sokhoyan, L. Zornberg, H. A. Atwater, *Adv. Mater.* **2017**, *29*, 1701044.
[19] Y. Takase, P. T. Thanh, R. Fujimura, K. Kajikawa, *Appl. Phys. Express* **2014**, *7*, 042202.
[20] S. Q. Li, X. Xu, R. M. Veetil, V. Valuckas, R. Paniagua-Domínguez, A. I. Kuznetsov, *Science* **2019**, *364*, 1087.
[21] I. C. Khoo, *Dig. Tech. Pap. - Soc. Inf. Disp. Int. Symp.* **2014**, *45*, 484.
[22] M. Decker, C. Kremers, A. Minovich, I. Staude, A. E. Miroshnichenko, D. Chigrin, D. N. Neshev, C. Jagadish, Y. S. Kivshar, *Opt. Express* **2013**, *21*, 8879.
[23] Y. Lee, M. K. Park, S. Kim, J. H. Shin, C. Moon, J. Y. Hwang, J. C. Choi, H. Park, H. R. Kim, J. E. Jang, *ACS Photonics* **2017**, *4*, 1954.
[24] O. Buchnev, N. Podoliak, M. Kaczmarek, N. I. Zheludev, V. A. Fedotov, *Adv. Opt. Mater.* **2015**, *3*, 674.
[25] M. Sharma, N. Hendler, T. Ellenbogen, *Adv. Opt. Mater.* **2020**, *8*, 1901182.
[26] L. Driencourt, F. Federspiel, D. Kazazis, L. T. Tseng, R. Frantz, Y. Ekinci, R. Ferrini, B. Gallinet, *ACS Photonics* **2020**, *7*, 444.
[27] M. L. Tseng, J. Yang, M. Semmlinger, C. Zhang, P. Nordlander, N. J. Halas, *Nano Lett.* **2017**, *17*, 6034.
[28] J. Olson, A. Manjavacas, T. Basu, D. Huang, A. E. Schlather, B. Zheng, N. J. Halas, P. Nordlander, S. Link, *ACS Nano* **2016**, *10*, 1108.
[29] I. C. Khoo, *Phys. Rep.* **2009**, *471*, 221.
[30] F. Simoni, *Nonlinear Optical Properties of Liquid Crystals and Polymer Dispersed Liquid Crystals*, World Scientific, Singapore **1997**.
[31] I. C. Khoo, *Liquid Crystals*, Wiley, Hoboken, NJ **2007**.
[32] H. K. Bisoyi, Q. Li, *Chem. Rev.* **2016**, *116*, 15089.
[33] I. C. Khoo, S. Zhao, *Prog. Electromagn. Res.* **2014**, *147*, 37.
[34] I. C. Khoo, *J. Opt. Soc. Am. B* **2011**, *28*, A45.
[35] S. G. Lukishova, *J. Nonlinear Opt. Phys. Mater.* **2000**, *09*, 365.
[36] I. C. Khoo, J. Liou, M. V. Stinger, S. Zhao, *Mol. Cryst. Liq. Cryst.* **2011**, *543*, 151/[917].
[37] L. Michaeli, D. B. Haim, M. Sharma, H. Suchowski, T. Ellenbogen, *Adv. Opt. Mater.* **2020**, *1*, 2000326.
[38] V. M. di Pietro, A. Jullien, U. Bortolozzo, N. Forget, S. Residori, *Laser Phys. Lett.* **2019**, *16*, 015301.
[39] S. A. Maier, *Plasmonics: Fundamentals and Applications*, Springer, New York **2007**.
[40] D. K. Yang, S. T. Wu, *Fundamentals of Liquid Crystal Devices*, Wiley, New Jersey **2014**.
[41] M. Shimizu, M. Sakakura, M. Ohnishi, Y. Shimotsuma, T. Nakaya, K. Miura, K. Hirao, *J. Appl. Phys.* **2010**, *108*, 073533.
[42] C. Umeton, G. Cipparrone, F. Simoni, *Opt. Quantum Electron.* **1986**, *18*, 312.
[43] G. Baffou, R. Quidant, *Laser Photonics Rev.* **2013**, *7*, 171.
[44] P. Berto, L. Philippet, J. Osmond, C. F. Liu, A. Afridi, M. M. Marques, B. M. Agudo, G. Tessier, R. Quidant, *Nat. Photonics* **2019**, *13*, 649.